



**HAL**  
open science

## Characterization of elastomers under simultaneous tension and torsion for application to engine mounts

Anne-Sophie Lectez, Erwan Verron, Bertrand Huneau, Franck Le Brazidec,  
Anne-Sophie Béranger

► **To cite this version:**

Anne-Sophie Lectez, Erwan Verron, Bertrand Huneau, Franck Le Brazidec, Anne-Sophie Béranger. Characterization of elastomers under simultaneous tension and torsion for application to engine mounts. ECCMR VIII, Jun 2013, San Sebastian, Spain. pp.603-608, 10.1201/b14964-108 . hal-04409047

**HAL Id: hal-04409047**

**<https://hal.science/hal-04409047>**

Submitted on 22 Jan 2024

**HAL** is a multi-disciplinary open access archive for the deposit and dissemination of scientific research documents, whether they are published or not. The documents may come from teaching and research institutions in France or abroad, or from public or private research centers.

L'archive ouverte pluridisciplinaire **HAL**, est destinée au dépôt et à la diffusion de documents scientifiques de niveau recherche, publiés ou non, émanant des établissements d'enseignement et de recherche français ou étrangers, des laboratoires publics ou privés.

# Characterization of elastomers under simultaneous tension and torsion for application to engine mounts

A.-S. Lectez, E. Verron, B. Huneau

*LUNAM Université, Institut de Recherche en Génie Civil et Mécanique (GeM), UMR CNRS 6183*

*École Centrale de Nantes, BP 92101, 44321 Nantes cedex 3, France*

A.-S. Béranger, F. Le Brazidec

*Direction Ingénierie Véhicule Renault, Direction de l'Ingénierie des Équipements et des Systèmes Châssis (DIESC)  
1, avenue du Golf, 78288 Guyancourt, France*

**ABSTRACT:** A general procedure is proposed to develop relevant multiaxial tension-torsion experiments that mimic the complex loading conditions undergone by engine mounts in service. First, displacements and forces exerted on the engine mount are measured on an instrumented vehicle. For several loading conditions, the displacements are introduced in a finite element model of the engine mount to determine the corresponding strain fields. To characterize and compare these strain fields, we consider the invariants of the Hencky strain tensor. For a given set of invariants, we determine displacements and angles that must be applied on the samples to reproduce the deformation of the engine mount. The present work focuses on the subsequent experimental campaign. Firstly, a new rubber specimen is designed for simultaneous tension-torsion tests. Its principal requirement is that the finite element strain field must be as close as possible to the analytical solution of the simultaneous extension and torsion of a cylinder. The geometry of the new sample is validated with the help of stereo digital images correlation (SDIC) on the lateral surface of the specimen. From SDIC results, relationships between global axial displacement and local extension  $\lambda$  on the one hand, and between global angle and local angle per unit of height  $\tau$  on the other hand are established. This validated method will be considered in a next future to perform multiaxial quasi-static and dynamic experiments, leading to identification of a visco-hyperelastic model.

## 1 INTRODUCTION

Due to the weight of the engine and various perturbations from the road, an engine mount in service undergoes several complex loading conditions. The non-linear elastic behavior of this elastomer part is commonly modeled by non-linear hyperelastic constitutive equations. Qualities required for a constitutive model are a small number of material parameters, a cover of the largest range of strain and being based on few simple tests (Steinmann et al. 2012). It was already highlighted that an identification of constitutive equations based on only uniaxial tension experiments fails to accurately predict others loading conditions (Seibert & Schöche 2000, Boyce & Arruda 2000, Attard & Hunt 2004, Marckmann & Verron 2006). In order to overcome these poor predictions, identifications are often enriched with several homogeneous experimental tests: compression or equibiaxial tests, pure shear, simple shear. Nevertheless, run-

ning all these tests is not an easy task since it requires different specimens and set-ups.

Covering up several loading conditions with a unique experimental set-up is simpler and allows to observe coupling between different strain states. Two principal types of multiaxial tests exist: biaxial tests with cross-shaped specimens (Rivlin & Saunders 1951, Blatz & Ko 1962, Treloar 1948, Kawabata et al. 1981, Becker 1967), and tension or compression combined with torsion using cylindrical specimens (Rivlin & Saunders 1951, Haupt & Sedlan 2001, Mars & Fatemi 2004, Suphadon et al. 2009). Few contributions have been found about tension/torsion tests, and those existing are mainly related to fatigue studies. In this case, the major requirement of the specimen is to present a stress concentration zone. As regards behavior characterization, the existence of a zone of interest in which the analytical solution for the mechanical problem is known takes precedence. The analytical solution of an infinite cylinder submitted to ten-

sion and torsion is known, but the specimen cannot be perfectly cylindrical since an effective interface with the testing machine has to be ensured. A compromise has to be found between the adequacy with the analytical solution and technical constraints. This question will be treated in the first part of this paper. In the second part, a method will be exposed to impose the local strain field during tension/torsion tests. This question is investigated by both Finite Element Analysis and Stereo Digital Image Correlation. It is to note that this experimental method is not often used for large strain problems (Chevalier et al. 2001, Meunier et al. 2008, Sasso et al. 2008, Sutton et al. 2008, Orteu 2009, Machado et al. 2010), and it is particularly rare for tension/torsion applications. It will result on the establishment of a relation between global angle and axial displacement applied by the machine on the specimen, and the local strain field in the zone of interest.

## 2 DESIGN OF THE SPECIMEN

### 2.1 Design criteria

The specimen is composed of mixture of carbon black filled natural rubber (NR) and styrene-butadiene rubber (SBR), close to the composition of the material used for engine mounts. The specimen design was steered by the following requirements, using the Instron ElectroPuls E10000 Linear-Torsion machine :

1. Ensure an efficient interface between jaws and specimen. Two aspects are concerned by this consideration: the type of mounting fixtures, which is driven by the geometry of existing jaw faces and the bonding between mounting fixtures and specimen.
2. Facilitate centering of the specimen in the testing machine.
3. Prescribe displacements within the linear stroke leading to large strains. Values to be reached are the maximum extension  $\lambda = 2.5$  and the maximum angle per unit of undeformed length  $\tau = 0.09 \text{ rad.mm}^{-1}$ .
4. Produce measurable torque and load, within sensors range.
5. Avoid instabilities.
6. Match the analytical solution of an infinite cylinder in an area of the specimen.

The major difficulty is to find a compromise between requirements 3 to 5, maximizing the size of the zone in which requirement 6 is met.

### 2.2 Kinematics

Figure 1 shows parameters for the tension-torsion of an homogeneous cylinder problem in the undeformed configuration. Deformation is supposed to remain isochoric. Equation 1 defines relations between deformed coordinates (small letters) and undeformed ones (capital letters), for a cylinder of initial length  $L$  submitted to an axial displacement  $u$  and an angle  $\phi$ .

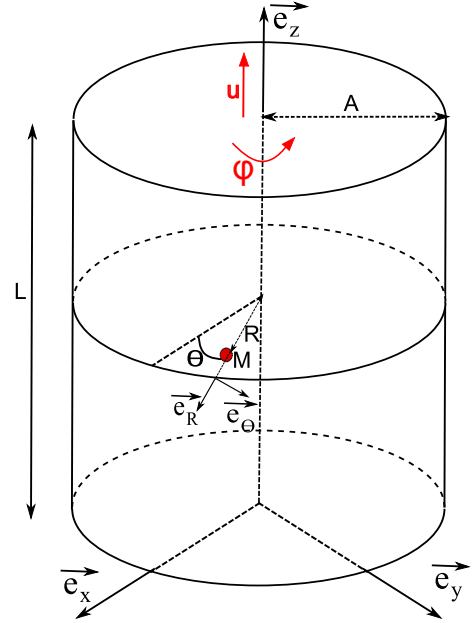


Figure 1: Variables used for describing the kinematics of a cylinder under tension and torsion

$$r = \frac{R}{\sqrt{\lambda}}, \theta = \Theta + \tau Z, z = \lambda Z \quad (1)$$

where  $\tau$  is the angle per unit of undeformed length and  $\lambda$  is the extension. Both parameters are position independent and equal to :

$$\tau = \frac{\phi}{L}, \lambda = \frac{l}{L} \quad (2)$$

### 2.3 Resulting geometry of the sample

The final geometry is composed of a cylindrical central zone, which radius and length have been fixed with respect to requirements 4 and 5 , largely widening at the ends (requirement 1). The ratio between total length and length of the cylindrical zone is driven by point 6. The steel mounting fixtures are cylindrical, allowing the use of Vee jaw faces. Their interfaces have been covered with adhesive and they have been inserted into the mold before the compression molding of the specimen (requirements 1 and 2). Figure 2 illustrates a 3D view of the specimen with its steel mounting fixtures.

In order to determine the zone in which strain is close to that calculated from the analytical solution of the infinite cylinder submitted to simultaneous tension and torsion, the principal values of Hencky strain



Figure 2: 3D view of the specimen and its steel mounting fixtures

tensor are calculated for the maximum loading conditions via Finite Element Analysis (FEA). Figure 3 shows the undeformed model geometry on which has been plotted the maximum principal strain values. This study is performed only on a quarter of the specimen, with axisymmetry. The constitutive model is a Mooney-Rivlin one, with material parameters identified by preliminary tension-compression tests.

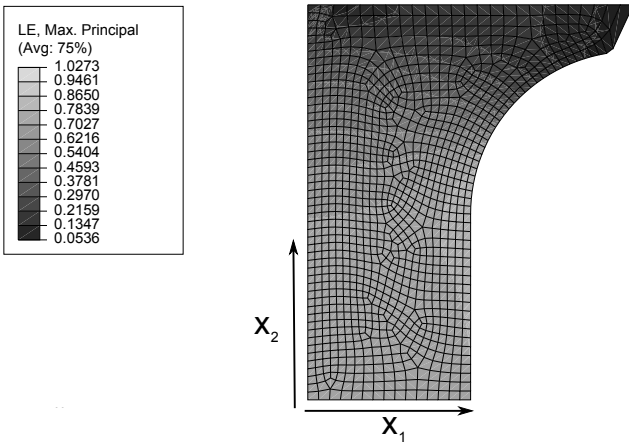
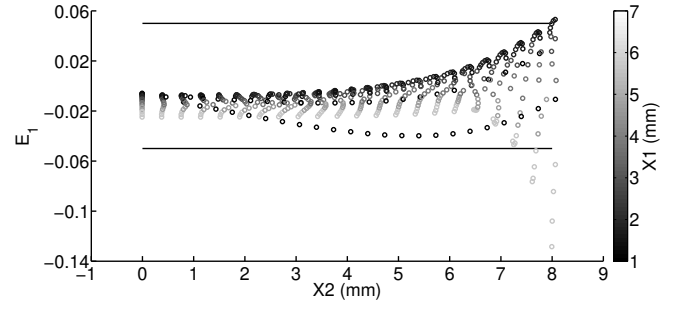
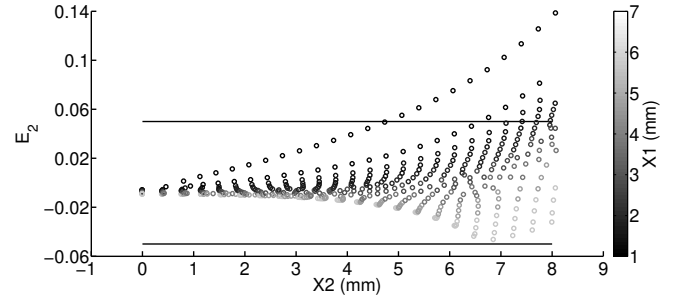


Figure 3: Maximum principal strain

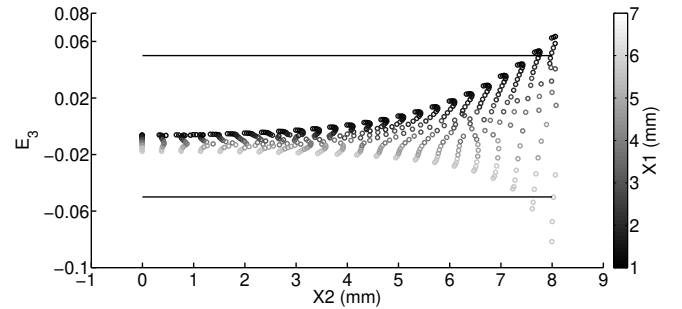
Along with this simulation, the analytical solution was calculated and compared with the results of FEA. Figure 4 illustrates the relative error for each principal strain against vertical nodes position. Gray shades are related to the radial position of nodes. Results are considered as similar if relative errors of all principal strains are less than 5%. Results are plotted only for nodes which are located in the central cylindrical zone. The 5% error is reached for the intermediate principal strain, for a vertical position which defines the length of the interest zone : 9 mm. On this zone, the mechanical problem will be assimilated to the mechanical problem of the infinite cylinder.



(a) Minimum principal strain



(b) Intermediate principal strain



(c) Maximum principal strain

Figure 4: Relative error between analytical solution and FEA for each principal strain. Straight lines represent maximum tolerated errors.

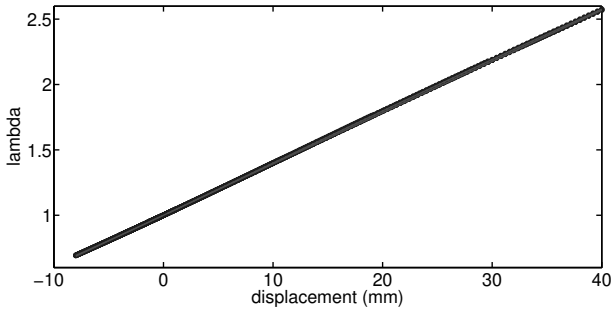
### 3 DETERMINATION OF LOADING CONDITIONS

Once strain values to be reached in the interest zone have been fixed, the corresponding global displacements have to be determined. If the specimen was perfectly cylindrical, this step would be obvious since Equation 2 determines this relation. Thus, as explained in the previous section, modifications had to be introduced and establishing relationships between  $u$ ,  $\phi$ ,  $\lambda$  and  $\tau$  is not straightforward due to heterogeneity.

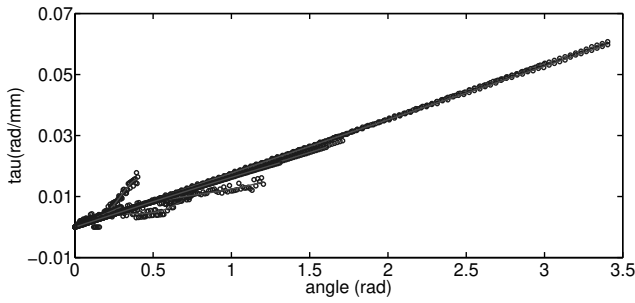
#### 3.1 Via FEA and analytical solution

Simulations with several couples  $(u, \phi)$  applied to the previous model are performed, computing strain in

the interest zone. Applying the kinematics of the infinite cylinder, couples of  $(\lambda, \tau)$  are calculated. Graphs of  $\lambda$  against  $u$  and  $\tau$  against  $\phi$  are shown in Figure 5. While the relation between  $u$  and  $\lambda$  is linear and independent of  $\phi$ , results about  $\tau$  are more complex: for large values of ratio  $u/\phi$ ,  $\tau$  is not linear with respect to  $\phi$ , while it does for all other cases. Besides, results depend significantly on the adopted constitutive model. Conclusions can hardly be drawn from this study, and further experimental investigations are needed.



(a) Local elongation  $\lambda$  against displacement  $u$



(b) Local angle per unit of undeformed length  $\tau$  against angle  $\phi$

Figure 5: Results of calculated  $\lambda$  and  $\tau$  for several couples  $(u, \phi)$

## 3.2 Via SDIC

Digital Image Correlation is an optical method which provides displacement fields tracking features position on several images. As the tracked surface is here a cylinder, two cameras are needed to provide out-of-plane displacements (Stereo Digital Image Correlation). Correlation is done by the software DaVis LaVision. The procedure is quickly described below.

### 3.2.1 Experimental set-up

Both cameras are placed close to the testing machine, about 40 cm from the specimen, with a  $20^\circ$  angle between them. A fine white speckle pattern is laid on the specimen, in order to create multiple shades of gray for image recognition. Cameras with same settings are synchronized to provide pictures of the specimen during tension and torsion at a fixed frequency, here 0.5 Hz.

### 3.2.2 Calibration

Firstly, indications about relative positions of both cameras and the filmed zone have to be given to the software. Pictures of a two depth levels calibration plate are made. White points, which position and size are known, are uniformly distributed over the plate. These points are recognized by the software. Based on points location in the local 2D coordinate system of each camera, the software rebuilds a global 3D coordinate system (Figure 6).

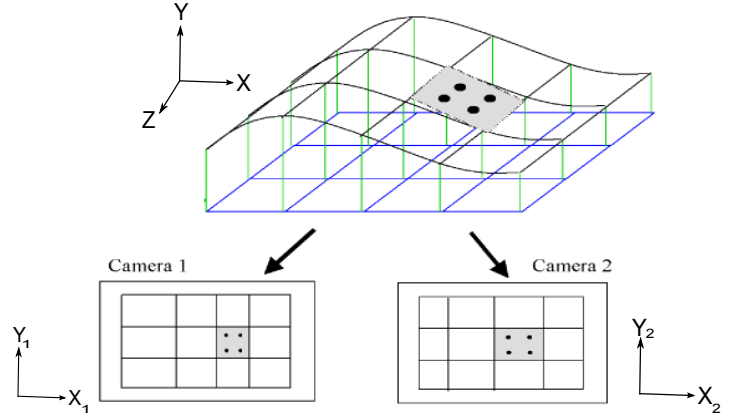


Figure 6: Reference coordinate systems of SDIC. Figure extracted from the product manual of DaVis 8.1.

### 3.2.3 Reconstruction of the surface and calculation of the displacement field

Once the calibration step is achieved, a picture of the undeformed specimen is taken by each camera. Using the calibration data, a 3D picture is reconstructed and discretized into a grid. Similarly, 3D pictures from the specimen at various deformation levels are rebuilt. Comparing the speckle pattern of the current state with the previous ones, the displacement field is calculated.

### 3.2.4 Post-processing

Errors made on undeformed and deformed positions are significant and data have to be filtered. This is particularly true for the out-of-plane coordinate corresponding to depth, and for deformation with high level of torsion. Points which are too far from the theoretical cylinder are suppressed and filters are applied to calculate  $\lambda$  and  $\tau$  through the relations :

$$\lambda = \frac{dz}{dZ}, \quad \tau = \frac{d\theta - d\Theta}{dZ} \quad (3)$$

### 3.2.5 Results

In order to present clear results, the chosen loading conditions consist in a simple axial displacement followed by torsion during which extension is maintained constant. Figure 7 illustrates the evolution of resulting  $\lambda$  and  $\tau$  during this test. Attention shall be paid to the heavy filters which had to be applied on the noisy data, leading to results with still significant

errors. As the objective here is indeed to access information about local quantities, post-processing including filtering, averaging or interpolating should be avoided as much as possible.

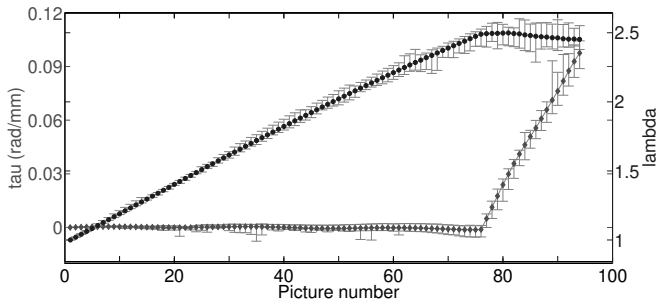


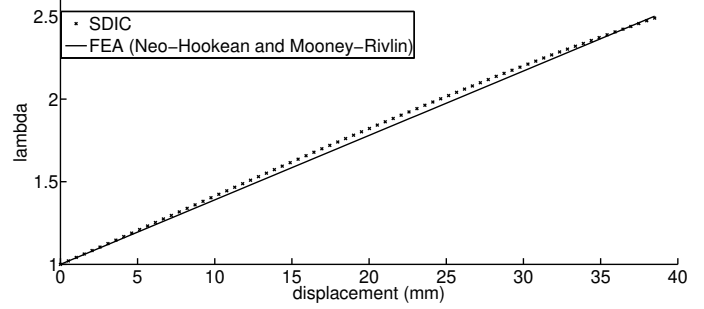
Figure 7: Evolution of  $\lambda$  (circles) and  $\tau$  (diamonds) during a two steps load: extension until picture number 76, then torsion with maintained extension. Error bars shows maximum and minimum values found at each state, after filtering

Figure 8 shows the comparison of results issued from SDIC and FEA. Concerning the evolution of  $\lambda$ , graphs are in good agreement, exhibiting a linear dependence on  $u$  with a similar slope. This result was quite expected, since FEA already gave stable results about  $\lambda$ , independently from  $\phi$  and the constitutive model. Results about  $\tau$  provide more information since same results have been found for several couples ( $u$ ,  $\phi$ ) with SDIC, unlike with FEA. To simplify the discussion, it has been chosen to report only the linear relation corresponding to the major part of the tested cases with FEA, excluding the non-linear curves. This linear relation has been calculated for two types of simple constitutive models, neo-Hookean and Mooney-Rivlin. Neo-Hookean model is quite close from SDIC result for low angles, and then overestimates it. Mooney-Rivlin model strongly underestimates SDIC results even at low angles. These models cannot be used to accurately predict the local angle per unit of length, which will probably be associated with inaccurate predictions of torsion curves.

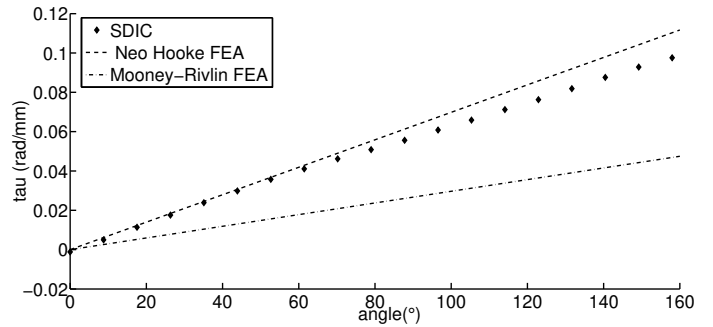
#### 4 CONCLUSION

An entirely dedicated to tension-torsion characterization specimen has been designed. This specimen guarantees good testing conditions as well as an efficient identification of constitutive models since it can be approximated by the analytical solution of an infinite cylinder. With the help of SDIC, we have been able to establish a simple relation between the axial displacement  $u$  and the local stretch ratio  $\lambda$ , and between the angle  $\phi$  and the local angle per unit of length  $\tau$ . Thanks to this experimental method, linear relations have been determined, rendering possible the prescription of given local strain through application of global displacement.

Based on these experimental relations, quasi-static tests will be performed in order to identify hyperelastic models. Preliminary studies indicate that sim-



(a) Evolution of  $\lambda$  against displacement  $u$



(b) Evolution of  $\tau$  against angle  $\phi$

Figure 8: Comparison of relations between  $\lambda, \tau, u$  and  $\phi$  using SDIC and FEA

ple models (neo-Hookean, Mooney-Rivlin) will fail to accurately predict multiaxial loading cases for large strains. Characterization will go further with a dynamic multiaxial campaign, which goal is to finally identify visco-hyperelastic models.

#### REFERENCES

- Attard, M. M. & G. W. Hunt (2004). Hyperelastic constitutive modeling under finite strain. *International Journal of Solids and Structures* 41(18-19), 5327–5350.
- Becker, G. (1967). On the phenomenological description of the nonlinear deformation behavior of rubberlike high polymers. *Journal of Polymer Science (Part C)*, 2893–2903.
- Blatz, P. J. & W. L. Ko (1962). Application of finite elastic theory to the deformation of rubbery materials. *Transactions of the Society of Rheology* 6(1), 223–251.
- Boyce, M. C. & E. M. Arruda (2000). Constitutive models of rubber elasticity: a review. *Rubber Chemistry and Technology* 73(3), 504–523.
- Chevalier, L., S. Calloch, F. Hild, & Y. Marco (2001). Digital image correlation used to analyze the multiaxial behavior of rubber-like materials. *European Journal of Mechanics - A/Solids* 20(2), 169–187.
- Haupt, P. & K. Sedlan (2001). Viscoplasticity of elastomeric materials: experimental facts and constitutive modelling. *Archive of Applied Mechanics (Ingenieur Archiv)* 71(2-3), 89–109.
- Kawabata, S., M. Matsuda, K. Tei, & H. Kawai (1981). Experimental survey of the strain energy density function of isoprene rubber vulcanizate. *Macromolecules* 14(1), 154–162.
- Machado, G., G. Chagnon, & D. Favier (2010). Analysis of the isotropic models of the mullins effect based on filled silicone rubber experimental results. *Mechanics of Materials* 42(9), 841 – 851.

- Marckmann, G. & E. Verron (2006). Comparison of hyperelastic models for rubber-like materials. *Rubber chemistry and technology* 79(5), 835–858.
- Mars, W. V. & A. Fatemi (2004). A novel specimen for investigating the mechanical behavior of elastomers under multiaxial loading conditions. *Experimental Mechanics* 44(2), 136–146.
- Meunier, L., G. Chagnon, D. Favier, L. Orgéas, & P. Vacher (2008). Mechanical experimental characterisation and numerical modelling of an unfilled silicone rubber. *Polymer Testing* 27(6), 765–777.
- Orteu, J.-J. (2009). 3-D computer vision in experimental mechanics. *Optics and Lasers in Engineering* 47(3-4), 282–291.
- Rivlin, R. S. & D. W. Saunders (1951). Large elastic deformations of isotropic materials. vii. experiments on the deformation of rubber. *Philosophical Transactions of the Royal Society A Mathematical Physical and Engineering Sciences* 243(865), 251–288.
- Sasso, M., G. Palmieri, G. Chiappini, & D. Amodio (2008). Characterization of hyperelastic rubber-like materials by biaxial and uniaxial stretching tests based on optical methods. *Polymer Testing* 27(8), 995–1004.
- Seibert, D. J. & N. Schöche (2000). Direct comparison of some recent rubber elasticity models. *Rubber Chemistry and Technology* 73(2), 366–384.
- Steinmann, P., M. Hossain, & G. Possart (2012). Hyperelastic models for rubber-like materials: consistent tangent operators and suitability for Treloars data. *Archive of Applied Mechanics* 82(9), 1183–1217.
- Suphadon, N., A. G. Thomas, & J. J. C. Busfield (2009). Viscoelastic behavior of rubber under a complex loading. *Polymer* 113, 693–699.
- Sutton, M., J. Yan, V. Tiwari, H. Schreier, & J. Orteu (2008). The effect of out-of-plane motion on 2D and 3D digital image correlation measurements. *Optics and Lasers in Engineering* 46(10), 746–757.
- Treloar, L. R. G. (1948). Stresses and birefringence in rubber subjected to general homogeneous strain. *Proceedings of the Physical Society* 60(2), 135–144.